2023-12-01

Ultrasonic Non-Destructive Evaluation Of Additively Manufactured Polymer-Ceramic Composites

Christian Alexander Ruiz
University of Texas at El Paso

ULTRASONIC NON-DESTRUCTIVE EVALUATION OF ADDITIVELY MANUFACTURED POLYMER-CERAMIC COMPOSITES

CHRISTIAN ALEXANDER RUIZ

Master's Program in Mechanical Engineering

APPROVED:

Yirong Lin, Ph.D., Chair

Jack Chessa, Ph.D.

Tommy Rockward, M.S.

Stephen L. Crites, Jr., Ph.D.

Dean of the Graduate School

ULTRASONIC NON-DESTRUCTIVE EVALUATION OF ADDITIVELY MANUFACTURED POLYMER-CERAMIC COMPOSITES

by

CHRISTIAN ALEXANDER RUIZ, B.S.

THESIS

Presented to the Faculty of the Graduate School of

The University of Texas at El Paso

in Partial Fulfillment

of the Requirements

for the Degree of

MASTER OF SCIENCE

Department of Aerospace & Mechanical Engineering

THE UNIVERSITY OF TEXAS AT EL PASO

December 2023

Acknowledgments

I would like to thank my advisor Dr. Yirong Lin for allowing me the opportunity to work with him and for his guidance these past three years. I would like to thank my friend and mentor Tommy Rockward for his great impact on my professional career and for allowing me to learn from him and improve myself as an engineer and scientist at Los Alamos National Laboratory. I would also like to thank my committee member Dr. Jack Chessa.

Thank you to all my colleagues and friends at Los Almos National Laboratory and the University of Texas at El Paso who helped make this work possible with all your hard work and guidance. Thank you, Gonzalo Seisdedos, Jabari Allen, Carla Navar, Jean Montes, Luis Rodriguez, and Stephanie Gonzalez.

Lastly, thank you to my friends and family for all their love and support and to Sofia Pinzon for the love, comfort, encouragement, and help, I could not have done it without any of you.

Abstract

Digital light processing (DLP) is an attractive additive manufacturing technique due to its ability to create ceramic parts with complex geometries. DLP uses ultraviolet light to polymerize a slurry comprised of ceramic powder and photosensitive resin in layers to create solid parts. Printing parameters such as light intensity and exposure time are critical when producing these parts. Improper parameters can lead to over or under-curing, adversely impacting print quality and strength. Samples were printed at varying layer exposure times and then tested using ultrasonics to determine the degree of conversion. Additionally, ultrasonics were used as a non-destructive technique to obtain the elastic modulus of the manufactured composites. The aim of this research was to investigate the effect of printing parameters on the ultrasonic response of polymer-ceramic composite parts and to establish a non-destructive method that incorporates ultrasonic techniques to evaluate mechanical properties to assure print quality.

Table of Contents

List of Tables

List of Figures

Table of Equations

1 Introduction

1.1 Motivation

Ceramics are essential to many industries and with the growing need for custom components, additive manufacturing (AM) offers the ability to produce ceramic parts that are not constrained by the geometrical limitations that plague traditional manufacturing techniques. The development of new resin slurries with varying compositions requires testing the resin with different print parameters to determine optimal settings. Print parameters influence the resolution, quality, and material properties of the AM parts. The degree of polymeric conversion is directly correlated to the print exposure time for DLP printing processes, and it also has a strong influence on the mechanical properties of the material. The current techniques to obtain the degree of conversion (DC) of polymers require the use of large, expensive equipment that is limited by its testing depth or must be done during active polymerization [1]. Material properties, such as the elastic modulus, of additively manufactured parts are measured using destructive techniques that ultimately destroy the part. This type of testing is not ideal since the same part would have to be reproduced each time for any additional testing resulting in higher costs, material waste, and longer manufacturing times. To mitigate this, nondestructive techniques such as ultrasonics can be used to test functional parts without destroying them and thus save time, money, and material. This work focuses on establishing non-destructive techniques, primarily utilizing ultrasonics, to test and characterize additively manufactured composites.

1.2 Background

1.2.1 Additive Manufacturing

Additive manufacturing is a novel manufacturing process that has transformed the way parts are designed and produced. Unlike traditional subtractive manufacturing methods that involve removing material from a solid block, additive manufacturing builds objects layer by layer. While traditional manufacturing methods often require complex tooling and molds that limit design options; additive manufacturing has the ability to create complex geometries, reduce material waste, and enable rapid prototyping [1] [2].

There are many kinds of additive manufacturing techniques and technologies, each with unique benefits and challenges. The current AM technologies (illustrated in Figure 1) have been categorized into the following seven classes: material extrusion, material jetting, binder jetting, powder bed fusion, direct energy deposition, sheet lamination, and vat polymerization [3]. Vat polymerization has advantages over other additive manufacturing techniques because of its high resolution, high dimensional accuracy, and ability to print with slurries that can be comprised of a variety of fillers and materials. Vat polymerization uses a projected light source and photopolymer resin to selectively cure layers to produce three-dimensional parts. The two main forms of vat polymerization techniques are digital light processing (DLP) and stereolithography (SLA). DLP works by projecting the full cross-sectional image of the layer using an ultraviolet (UV) projector for a set amount of time. The ability to effortlessly control the photopolymer's time under UV makes it practical for applications that include the development of resins and slurries. SLA is a similar process to DLP but rather than projecting the full image of each layer at once, SLA uses a laser to scan across the surface.

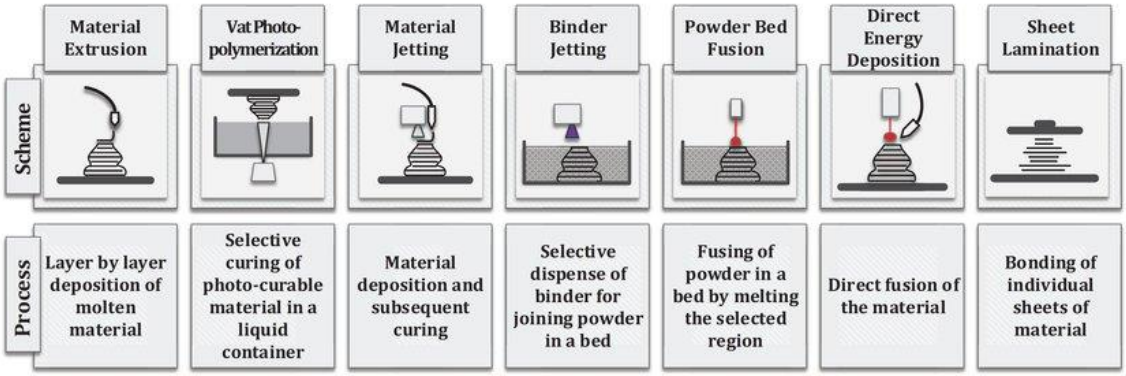

Figure 1: Current additive manufacturing methods [4]

Photopolymer resin used in DLP printing is made up of oligomers, monomers, and photoinitiators. Photoinitiators convert the photolytic energy into reactive species that cause cross-linking of the oligomers and monomers when exposed to ultraviolet wavelength light. This reaction is demonstrated in Figure 2 [5]. The crosslinking creates polymer chains that form solid layers that reiterate layer by layer [6]. The degree of conversion is the extent to which the polymer chains are created from the crosslinking of monomers. It can be varied by controlling the dose of the UV light, such as intensity and exposure time [7]. Conversion can be observed as the C=C double bonds convert to C-C single bonds [8]. The DC is important because it helps determine the material properties of polymers such as mechanical strength [9] [10]. Suboptimal curing parameters also influence the surface quality leading to a lower resolution of features on the print.

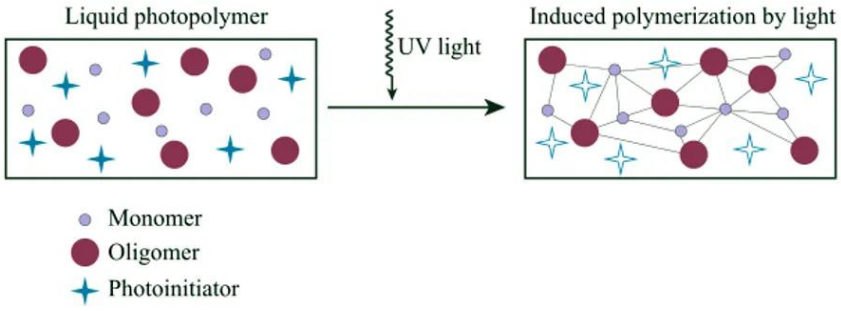

Figure 2: Polymerization process [11]

The theoretical trend for the degree of conversion would expect a rapid increase in polymerization followed by a dramatic slowing down of the reaction as seen in Figure 3 [12]. This trend was observed by Wu et al. in free radical polymerization of photopolymers in real time using Fourier transform infrared spectroscopy (FTIR) and supported by their model for monomer conversion [12].

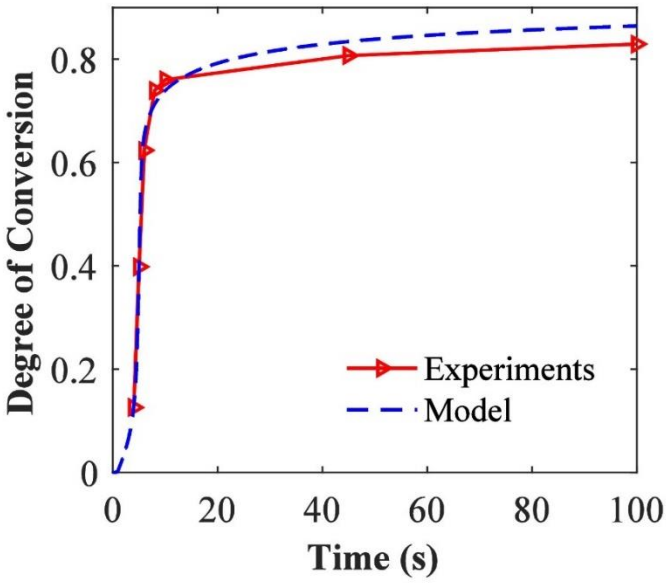

Figure 3: Photopolymer degree of conversion model compared with FTIR [12].

1.2.2 Advanced Ceramics

Advanced ceramics are made from inorganic compounds with higher purities than organic ceramics [13]. Ceramics offer a wide range of benefits across various industries and applications. One of the key advantages of ceramics is their exceptional heat resistance, which makes them ideal for high-temperature environments such as furnaces, engines, and aerospace components [14]. Ceramics possess excellent electrical insulation properties, crucial in electronic and electrical applications [15]. Properties such as hardness and wear resistance make ceramics invaluable for manufacturing cutting tools, bearings, and armor materials [16]. The biocompatibility of ceramics makes them suitable for use in medical applications. Ceramics are known for their corrosion resistance, which extends their lifespan in harsh chemical environments [17].

Advanced ceramics are polycrystalline materials that are generally divided into metal oxides like alumina (Al_2O_3) and zirconia (ZrO_2), and non-oxides [13]. Alumina is a popular advanced ceramics mainly because of its abundance and availability [15]. Alumina, and most other ceramics, are typically manufactured using dry-forming and wet-forming manufacturing methods. Dry forming uses dry ceramic powders and compresses them to form a solid piece [18]. Wet forming involves mixing a ceramic powder with a binder or heating the material until molten, the material is then extruded or injected into a mold [18]. The main limiting factors for these manufacturing processes are the complexity and geometry of the part. Additive manufacturing offers a solution to create ceramic parts that are not limited by traditional manufacturing geometry constraints. Figure 4 shows the complex ceramic parts and lattices manufactured using vat polymerization by Liu et al. [19].

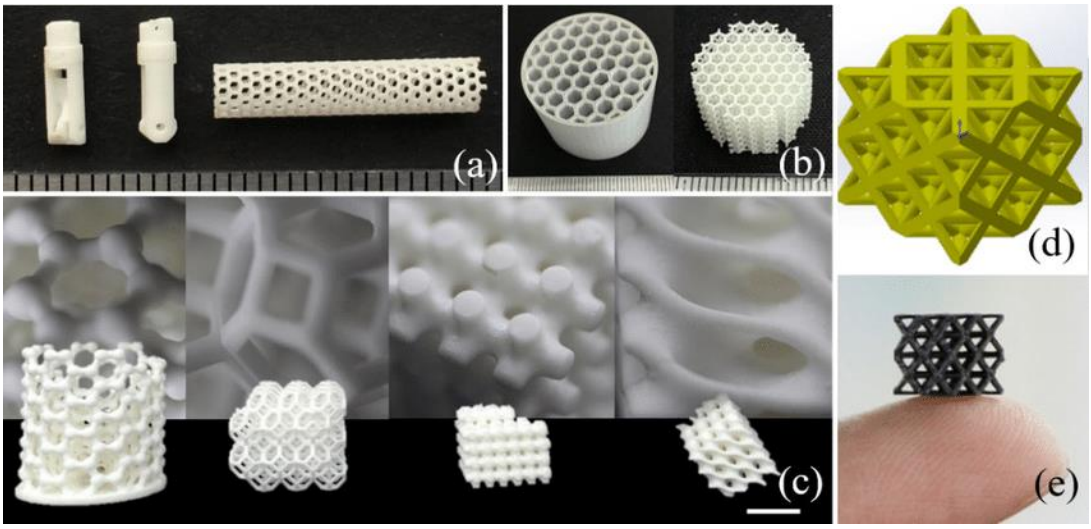

Figure 4: Ceramic parts manufactured using vat polymerization AM techniques by Liu and Chen [20].

Additive manufacturing of ceramics using vat polymerization techniques requires the use of a photopolymer binder to suspend the ceramic to print. The printed ceramic part leaves the printer as a green part which must go through thermal post processing to obtain a pure ceramic part [20]. The polymer-ceramic green part is an additively manufactured part before it undergoes post processing, in this case it is made up of powdered ceramic in a polymer matrix. Thermal post processing is performed to remove the polymer binder from the part to leave only the ceramic, this is accomplished by putting the print in a high temperature oven to burn out the polymer and sinter the ceramic [21]. The end result part shrinks due to loss of mass and volume from the polymer removal, resulting in a solid ceramic piece.

1.2.3 Non-Destructive Testing

Non-destructive testing (NDT) is a critical methodology used across various industries to assess the integrity, quality, and material properties of components without causing any damage

or affecting their functionality [22]. NDT techniques encompass a diverse range of methods (illustrated in Figure 5) such as ultrasonic testing (UT), radiographic testing (RT), magnetic particle testing (MT), and visual inspection (VT), among others [22]. These methods allow for the detection of defects or flaws in materials, providing valuable insights into their reliability and performance. NDT plays a pivotal role in ensuring the safety of critical infrastructure as well as in quality control processes for manufacturing industries, including aerospace, automotive, and construction [23]. NDT contributes significantly to maintaining safety standards, reducing maintenance costs, and ensuring the longevity of components and assets by enabling the identification of material properties and detection of hidden flaws and defects [23].

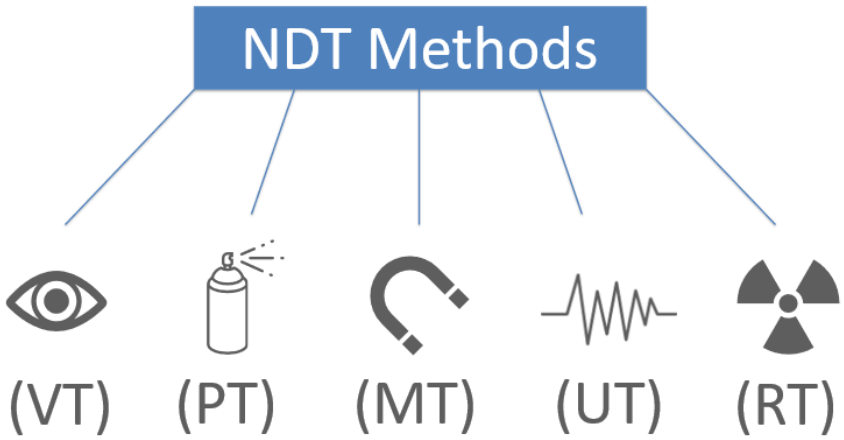

Figure 5: Five most common NDT methods.

Ultrasonic testing involves the use of high-frequency sound waves, typically beyond the range of human hearing, to detect internal flaws or defects within an object as well as give insight into the material properties [1] [24]. Ultrasonic transducers generate sound waves and direct them into the material being tested. The time of flight (ToF) is recorded by observing the time it takes for the waves to pass through the material as shown in Figure 6. When the sound

waves encounter a boundary or defect within the material, they are reflected to the transducer or picked up by a receiving transducer allowing for its detection. The size, location, and nature of any flaws present, such as cracks, voids, or inclusions can be determined by analyzing the ToF of the echoes and their amplitude [25].

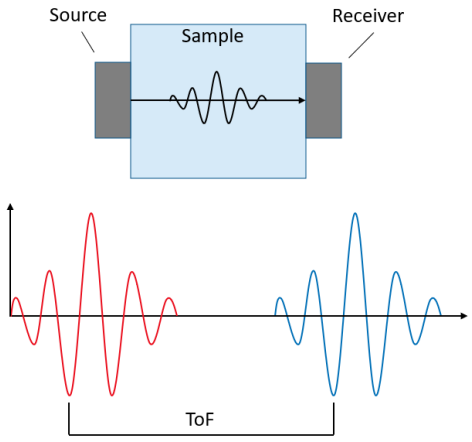

Figure 6: Ultrasonic testing diagram to obtain time of flight.

The acoustic properties of polymers are related to many of their structural properties such as morphology, transition temperature, and cross-link density [26]. For isotropic polymers, the two wave modes of acoustic propagation are longitudinal waves and shear waves. Longitudinal mode has a particle motion that is normal to the surface and has a compression effect [26]. Shear mode particle motion is perpendicular to the wave's direction of propagation [26].

2 Experimental Design and setup

2.1 Equipment and Materials

The DLP printer used for this work was a Bison 1000 printer by Tethon 3D (Nebraska, United States). The Bison 1000 prints at a wavelength of 406 nm and has a pixel size of 57 µm with a projector screen resolution of 1920 x 1080 pixels and a maximum build volume of 110 x 60 x 138 mm. The base resin used for 3D printing of parts was Genesis High Load by Tethon 3D. This resin was used because it is a developmental resin with a low viscosity that can accept large amounts of powder filler such as alumina in the case of this project. The alumina (Al_2O_3) powder that mixed into the base resin had a particle size of 350 nm and was purchased from Inframat Advanced Materials (Connecticut, United States). BYK-W 9010 surfactant, manufactured by BYK ALTANA (Wesel, Germany), was mixed into the resin-powder slurry using a Thinky ARM-310 high shear planetary mixer (Thinky California, United States) to ensure that the alumina particles were evenly suspended. A Form 3 Stereolithography printer was used to manufacture parts using Clear V4 resin (Formlabs, Massachusetts, United States). The Form 3 has a resolution of 24 µm and a laser spot size of 85 µm with a build volume of 145 x 145 x 185 mm.

The ultrasonic testing setup included an AFG3022C function generator and MDO32 mixed domain oscilloscope by Tektronix (Oregon, United States). The function generator is equipped with dual channels capable of operating up to 25 MHz with a 20 V amplitude into 50 Ω loads. The MDO32 2 channel oscilloscope is operational up to 1 GHz with a sample rate up to 5 GS/s. The ultrasonic testing setup also included longitudinal (V133-RM 2.25 MHz) and shear (V154-RM 2.25 MHz) wave transducers to convert the electrical signals to acoustic-mechanical signals. The transducers used in the setup were purchased from Olympus (Tokyo, Japan) and were ideal for this application because of their peak operating frequency of 2.25 MHz.

Mechanical testing was performed using an Intron® 6800 (Intron®, Massachusetts, United States) that has a force capacity of 100 kN. Strain was measured during mechanical testing using an Epsilon ONE® optical extensometer (Epsilon®, Wyoming, United States). The optical extensometer had an operating resolution of <0.5 µm quasistatic, <2.5 µm dynamic, <0.1 µm creep, which makes it ideal for measuring small changes in strain. FTIR tests were performed using a Nicolet™ iS™ 10 (Thermo Fisher Scientific, Massachusetts, United States). A MakerBot Mark3 (MakerBot, New York, United States) fused deposition modeling printer was used to manufacture experimental setup support parts and components using the Tough Precision Model Material filament.

2.2 Resin Ceramic Slurry Procedure

Ceramic alumina powder was weighed out and added to the Genesis High Load resin according to desired ceramic loading by weight percent, two resin slurries were produced: a 20 wt% and 40 wt% alumina to resin. Genesis High Load is a developmental photopolymer resin with a low viscosity able to accept a large quantity of solid loadings. BYK-W 9010 surfactant was added at 2% of the total mass of the slurry to help slow sedimentation and resist agglomeration of ceramic particles. BYK-W 9010 is a wetting and dispersing additive for polymer systems, its functionality comes from its phosphoric acid esters making it an anionic surfactant [27] [28]. After the constituents of the ceramic resin slurry were combined, the slurry was placed in the Thinky ARM-310 and mixed at 2000 rpm for 3 minutes.

2.4 Ultrasonic Testing Setup

The ultrasonic testing setup (illustrated in Figure 8) is comprised of a function generator, an oscilloscope, and a set pair of longitudinal and shear wave transducers. The function generator outputs an electrical signal which is transmitted through one lead that goes to a transducer and

another that goes into the oscilloscope to be used as a baseline excitation signal. Additionally, a trigger cable is linked to the oscilloscope from the function generator to synchronize the horizontal signals to prevent shifting of the signals during testing. The printed samples were sandwiched between two ultrasonic transducers: the source (output) transducer and the receiver (input) transducer. The source transducer is connected to the function generator to convert the electrical signals into acoustic waves while the receiver converts the resulting acoustic waves through the sample back into electrical signals and relays them to the oscilloscope. The resulting signals obtained with the receiver are displayed and recorded on the oscilloscope.

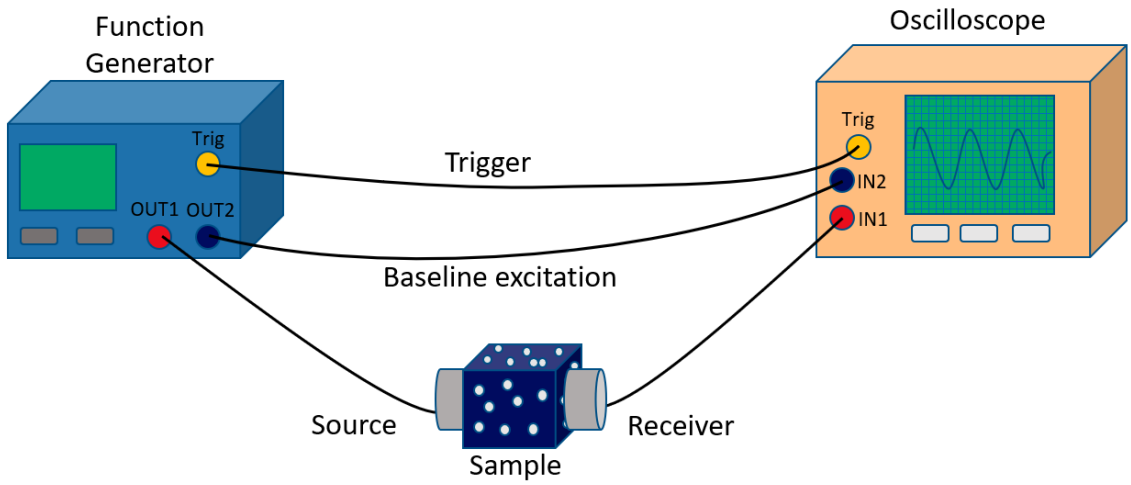

Figure 7: Ultrasonic testing setup diagram.

The function generator was set to output a 5-cycle burst sinusoidal waveform with a 10 V peak to peak amplitude and a set frequency to channel 1 (the source transducer). A 1 V peak to peak signal with the same waveform was output to channel 2 as the baseline excitation. The frequency set was dependent on the type of ultrasonic test being performed. A single frequency of 2.25 MHz was used for DC testing of samples cured at varying exposures. The ultrasonic technique employed to test the mechanical properties utilized a frequency sweep with a step size

of 0.1 MHz and frequency ranges (listed in Table 3) depending on the material's acoustic attenuation.

Table 1: Ultrasonic frequency sweep ranges per sample type.

Sample Type	Longitudinal Frequency Range (MHz)	Shear Frequency Range (MHz)
Formlabs Clear	2.3-2.7	1.5-1.9
20%	2.2-2.6	1.7-2.1
40%	2.2-2.6	1.0-1.4

2.4 Density Calculation

Often ultrasonics measurements require some fundamental knowledge of the samples. The density of the manufactured parts must be known to calculate their material properties using ultrasonics. The density of the samples was calculated using Archimedes' principle of density, which states that the weight of the fluid displaced is equal to the buoyant force acting on the part [30]. The parts were weighed in air and then weighed again while submerged in a liquid with a known density to determine the density of the part. An apparatus was designed in Autodesk® Fusion 360™ and manufactured using the MakerBot Method to weigh the mass of the part submerged in water without the mass of the water imposing on the mass balance, the design and setup can be seen in Figure 9. Equation 1 was used to calculate the density where $\boldsymbol{m_{Dry}}$ is the mass of the object dry, $\boldsymbol{m_{Wet}}$ is the mass of the object submerged in a fluid, and $\boldsymbol{\rho_{Fluid}}$ is the density of the fluid. This technique to determine the density of the part considers any vacancies within the manufactured parts.

$$\rho = \frac{m_{Dry} \cdot \rho_{Fluid}}{m_{Dry} - m_{Wet}}$$

Equation 1: Archimedes' principle density formula.

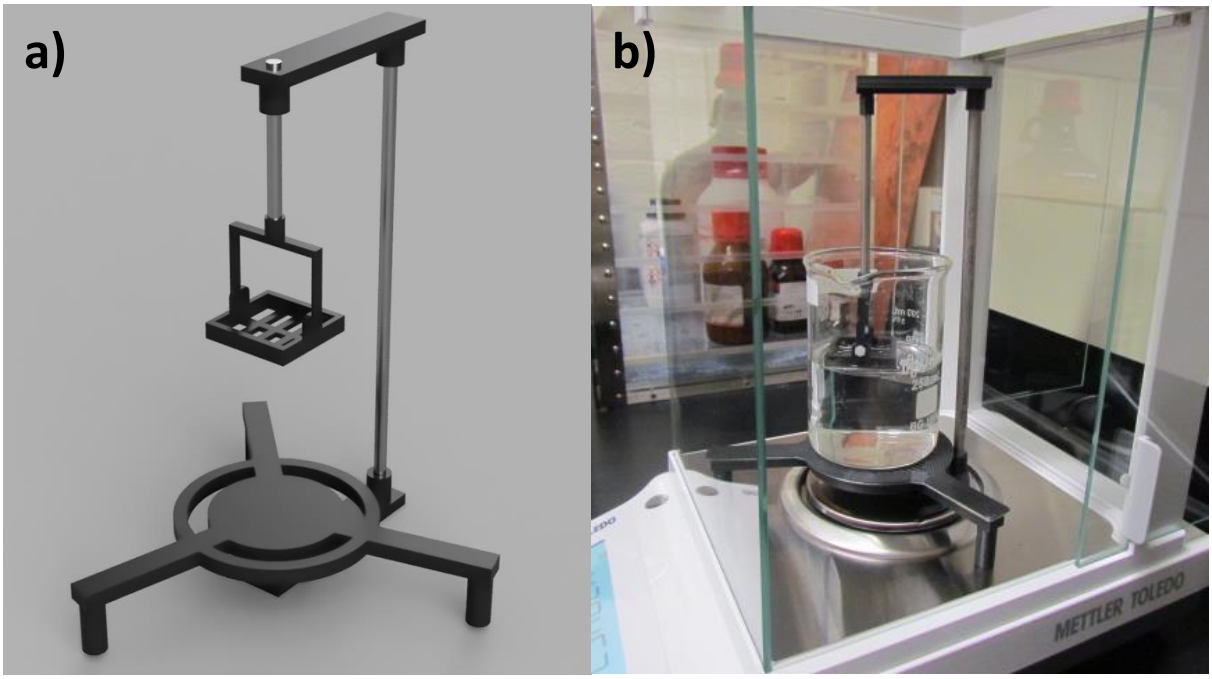

Figure 8: a) CAD drawing of Archimedes' density apparatus. b) Archimedes' principle testing setup.

2.3 AM Printing

A Bison 1000 DLP printer was used to print the polymer ceramic parts and a diagram for the DLP printing process can be seen in Figure 7. Prior to printing, calibration was needed to ensure the build plate lies flush with the vat screen. This was done by lowering the build plate to the bottom of the tank and leveling the plate to the tank film screen. The slurry was mixed prior to printing at 2000 rpm for 2 minutes to ensure uniformity and dispersion of the ceramic particles. The slurry was poured into the vat and the print parameters were selected. The layer height resolution was set to 0.05 mm and the prints were manufactured at ambient temperature (18-24°C). The print exposure times were input into the printer depending on the test and filler

weight percent then the prints executed. The finished green part was then washed in isopropyl alcohol to remove any uncured resin from the surface and placed in a UV oven for 5 minutes to continue to cure the surface and to remove any tacky surface finish. Only UV post processing was applied to the parts, thermal post processing was not required for this work given that its application is for polymer-ceramic composites.

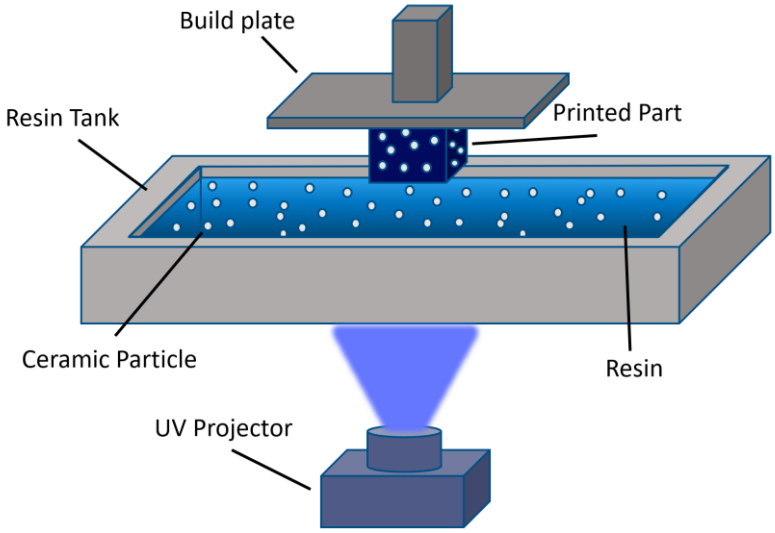

Figure 9: DLP printing diagram.

The most important print parameters on the Bison 1000 printer are the following: layer height, light intensity, basic exposure, initial exposure, initial exposure layers, basic layer wait time, and initial layer wait time. The layer height is the height step per layer, this value influences the resolution of the print in the Z-axis. The light intensity is a unitless value given by Tethon that represents the range of brightness of the projector. The basic and initial exposure parameters determine the amount of time each layer is exposed to the UV light. The layer wait time is the delay between each successive layer, the delay is necessary to allow the liquid resin to flow over the vat screen, with more viscous resins requiring a longer delay. The initial layers

make up the first few layers, it is typical for these layers to have higher exposure times to allow for good adhesion to the build plate. The basic layers make up most of the print.

The exposure times for each printed part varied from 17 to 100 seconds while layer wait times, number of initial layers, and light intensity were held constant. The print time was varied to gauge the degree of conversion with respect to the time under UV and to identify optimal print exposure times. The print parameters for these tests are listed in Table 1. The print parameters for developmental resins must be determined by the user since the parameters are dependent on factors like the filler type and concertation, along with any additives used. It is recommended to conduct test prints when using developmental resins to help establish the appropriate parameters.

Table 2: Print Parameters for DC Test Samples at 20 wt% alumina filler at a light intensity of 170.

Basic Exposure (s)	Initial Exposure (s)	Initial Exposure Layers	Basic Layer Wait (s)	Initial Layer Wait (s)
17	20	4	30	20
30	30	4	30	20
45	45	4	30	20
60	60	4	30	20
80	80	4	30	20
100	80	4	30	20

The ceramic filler amount was varied for the next sample set which was used to determine the mechanical properties. The change in filler loading was to observe the effect of the ceramic particles on the mechanical properties of the composites and to determine whether the elastic modulus could successfully be deduced using ultrasonic techniques no matter the constituents and their concentration in the polymer matrix. Three sample types were

manufactured for these tests with varied filler mass ratios: 0% (no filler), 20%, and 40%. The developmental resin used for the slurries is intended for mixing with dry powders and is not meant to be printed on its own as stated by the manufacturer [29]. For this reason, the samples without filler (0%) were manufactured using Formlabs Clear resin and printed using a Form 3 SLA printer. The print parameters and settings for the Clear resin are not made available by the manufacturer.

Table 3: Print Parameters for Mechanical Properties Test Samples at a light intensity of 170.

Filler wt%	**Basic Exposure**	Initial Exposure (s)	Initial Exposure Layers	Basic Layer Wait (s)	Initial Layer Wait (s)
Clear	NA	NA	NA	NA	NA
20	60	60	4	30	20
40	120	140	4	30	20

3 Ultrasonic Verification of Degree of Conversion

3.1 Intro

The degree of conversion is one of the most important parameters that affect the mechanical properties of polymer composites [31]. Typical methods to determine the DC include FTIR and differential scanning calorimetry (DSC), both requiring large, expensive pieces of equipment. This work proposes a technique to determine the DC of the printed parts using ultrasonics.

3.2 Results and Discussion

3.2.1 Ultrasonic Response

The ultrasonic response of the samples was recorded using the longitudinal transducers at 2.25 MHz. Figure 10 shows an example wave data set where the shift in the sample signal with respect to the baseline excitation signal can be observed. Channel 1 is the signal through the sample while channel 2 is the baseline excitation. The shift in the signal through the sample is used to obtain the ToF, which is the time it takes for the acoustic wave to travel through the sample. The ToF was measured using a cross-correlation function. The correlation function, shown in Equation 2, measures the strength of the relationship of two signals and outputs the correlation coefficient [32]. MATLAB was used to process the data and output a correlation plot to determine the highest correlation coefficient (Figure 11). The data point with the highest correlation factor is then used to determine the signal lag. The signal lag is converted to ToF using the data acquisition rate of the oscilloscope.

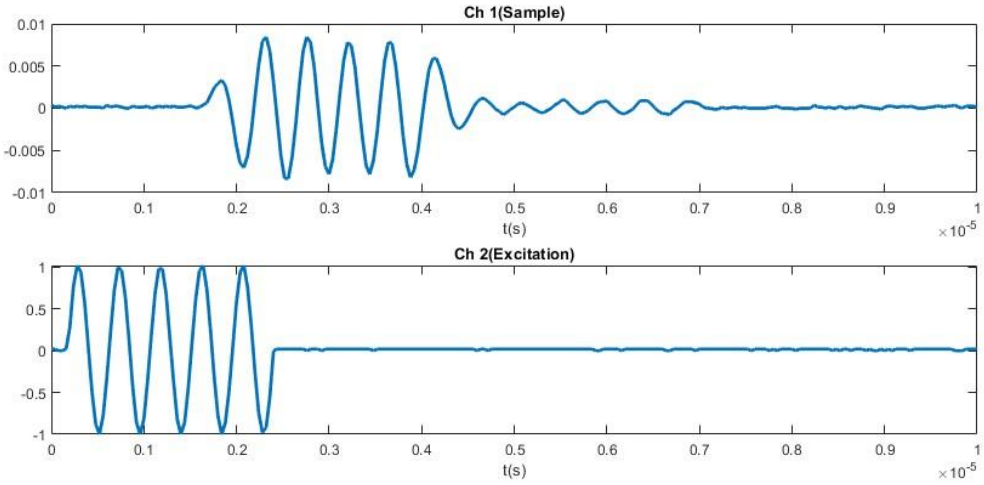

Figure 10: Ultrasonic sample waveforms.

$$\boldsymbol{Correlation(g,h) = \int_{-\infty}^{+\infty} g(\tau + t)h(\tau)d\tau}$$

Equation 2: Correlation Function.

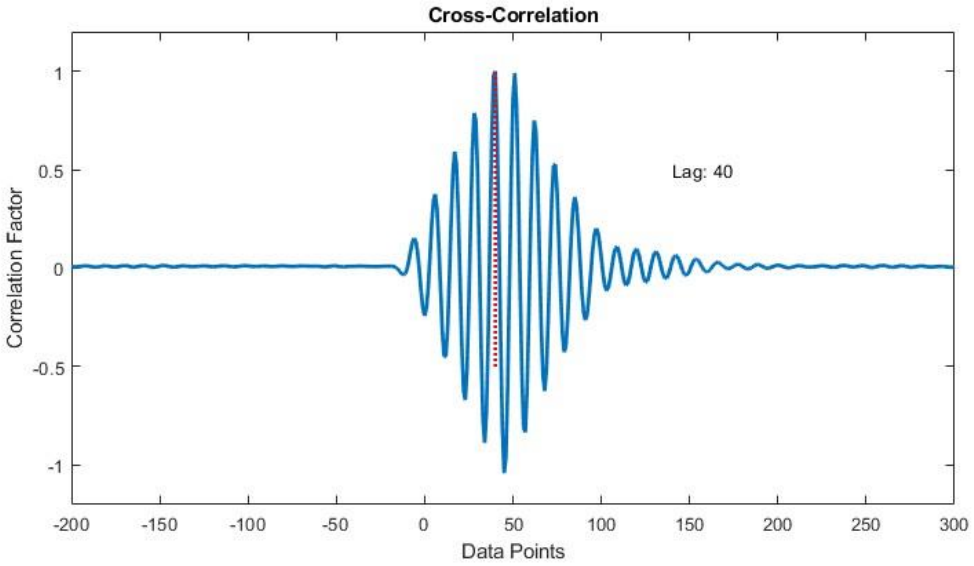

Figure 11: Cross-Correlation Plot.

3.2.2 Ultrasonic Velocity

The ultrasonic velocity through the sample was calculated using Equation 3ftir where *t* is the thickness of the sample between the two transducers and ToF is the time of flight. The ultrasonic velocities show an asymptotic behavior that started with large a slope and then leveled out. The acoustic velocities with respect to exposure time for the printed samples can be seen in Figure 12 a). The slowest sound velocity observed was 1620.65 m/s, which belonged to the sample with the lowest exposure time of 17 seconds. The sample with the highest exposure time of 100 seconds also exhibited the highest ultrasonic velocity of 1817.31 m/s. Figure 12 b) shows the rate of change between each printed sample as exposure time was increased. By increasing the exposure time from 17 to 30 seconds, a 9% increase in ultrasonic velocity was observed whereas only a 3% increase in ultrasonic velocity was observed when increasing the exposure time from 30 to 100 seconds. This trend supports the theoretical trend of the degree of conversion for polymers, a rapid conversion followed by a region where the conversion slows down drastically as seen in the data from Wu et al. and Figure 3 [12].

$$\boldsymbol{V = t/ToF}$$

Equation 3: Acoustic Velocity through a solid.

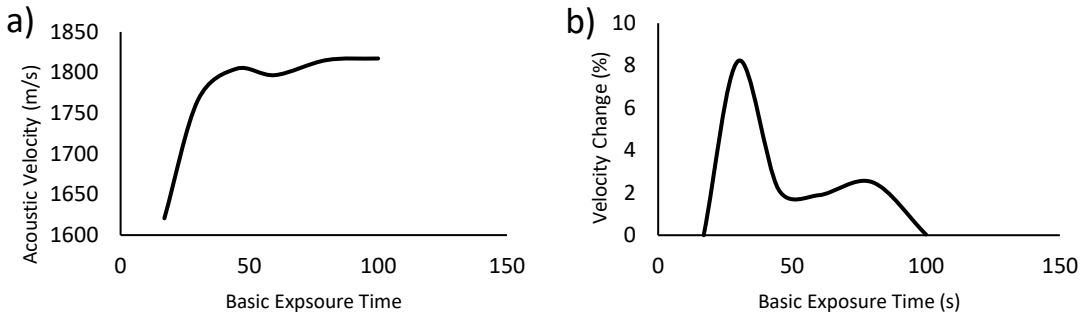

Figure 12: a) Average acoustic velocity with respect to basic layer exposure time. b) The velocity percentage change with respect to basic layer exposure time.

The reaction kinetics for free radical photopolymerization reactions begin with rapid conversion and then slow down. As the reaction takes place and the slurry transitions to a glassy state, the polymerization kinetics are affected due to the reduction in the mobility of the monomers, oligomers, and the reacting radicals [34]. The crosslinking density of photopolymers is linked to the exposure time, as the exposure time increases it allows more time for the reactive species to interact with the monomers and oligomers until an eventual slowing down of the reactions. The polymerization stalls despite the presence of unpolymerized monomers and radicals [34]. The crosslinking density of polymers has a considerable influence on the material's mechanical properties [35]. The ultrasonic response of a material is tied to its mechanical properties; therefore, the degree of conversion can be seen as the change of the material properties as observed by the change in acoustic velocity through the medium.

3.2.3 FTIR

Fourier transform infrared spectroscopy is a powerful technique that allows for the observation of chemical bonds and properties using infrared light. FTIR is a technique used to determine the degree of conversion for polymers as it can observe chemical bonds associated with polymerization. For polymers, the degree of cure is observed by the C=C bonds at 1620

cm^{-1} and 1635 cm^{-1} [12]. error. The FTIR data collected for each sample, shown in Figure 13, was normalized with respect to the C=O stretching vibration peak at 1725 cm^{-1}.

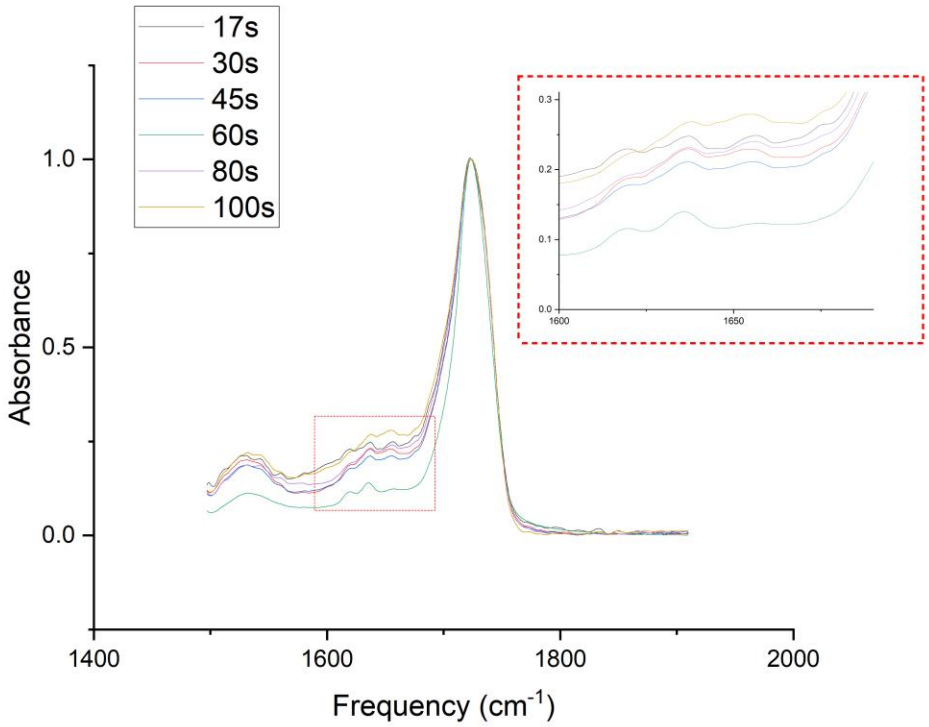

Figure 13: FTIR spectrum of samples manufactured at varying light exposure times.

The samples that were used in the ultrasonic technique were also tested using FTIR spectroscopy to confirm if a trend in the absorbance peaks associated with the double bond conversion could be used as an indicator of polymerization. There was no visible trend in the C=C peaks with respect to the exposure time. The lack of a trend could be in part due to the scanning depth of the FTIR. The samples tested were UV post processed, a typical procedure when additively manufacturing photopolymer parts, this surface treatment does penetrate the part to some extent depending on the opacity of the part. The parts were also exposed to ambient light conditions during the ultrasonic testing. Both the UV post processing and exposure to ambient

light continue the polymerization and may continue to cure past the scanning depth of the FTIR system which is in the micrometer range [36].

FTIR spectroscopy was performed on single-layer prints and uncured resin slurry to test whether the lack of an observable trend in the absorbance peaks was due to the UV post processing and exposure to ambient light. The single-layer prints were manufactured using the 20% alumina resin, rinsed with IPA, and stored in a dark environment to be tested the following day using FTIR. Unlike the previous set of samples tested, the single-layer prints were not post cured and experienced less time between manufacturing and testing to reduce external influences on the degree of conversion of the part. Figure 14 shows a visible trend with the C=C absorbance peaks decreasing as the light exposure time increases.

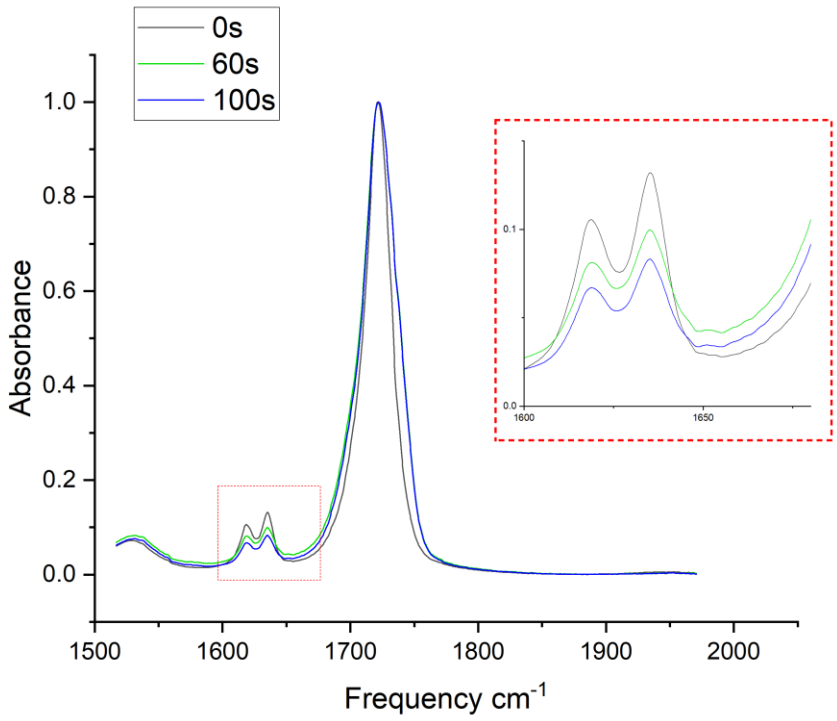

Figure 14: FTIR spectrum of single-layer print samples manufactured at varying light exposure times with minimal light exposure between printing and testing.

3.2.4 Validation Matrix

A printing validation matrix is a test print geometry designed to assist in the calibration to determine the print parameters for optimal surface resolution. Curing the print layers for too long will result in light scattering which leads to a loss of resolution. On the other hand, under-curing can also result in loss of resolution due to inadequate time needed to properly polymerize. Both over and under-exposure will lead to dimensional inaccuracies. A validation print has geometries and surface features that make evident any inaccuracies of the print to the user. Matrices were printed with parameters to coincide with the basic exposure times of the printed parts used for the ultrasonic degree of cure test. A separate validation test geometry was needed since the printed samples were very simple and had no surface features to help distinguish the quality of the prints with respect to the parameters. The validation matrix used was the Resin XP2 Validation Matrix (Figure 15) created by Photononsters.

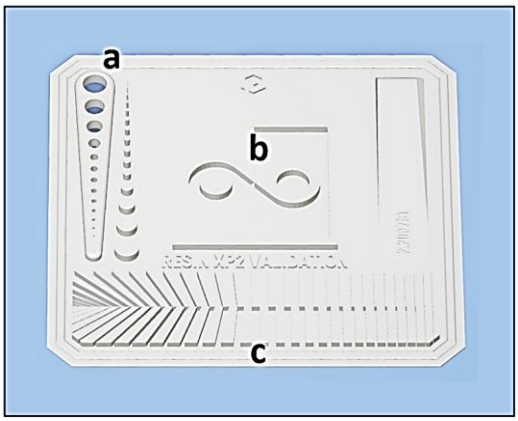

Figure 15: Validation matrix by Photonsters.

Figure 16 shows the results of the validation matrix with respect to the change in the exposure time. The main features of interest on the validation matrix are the holes and the pins on the right side of the print (a), the two halves of the infinity sign in the center (b), and the bars

and slots located at the bottom (c), as seen on Figure 15. The holes develop as the exposure time increases from 17s to 100s. Slight over-exposure can be seen at 100s as evident from the bars and slots, the bars should fit in the lower slot section, this dimensional inaccuracy is a sign of over-curing.

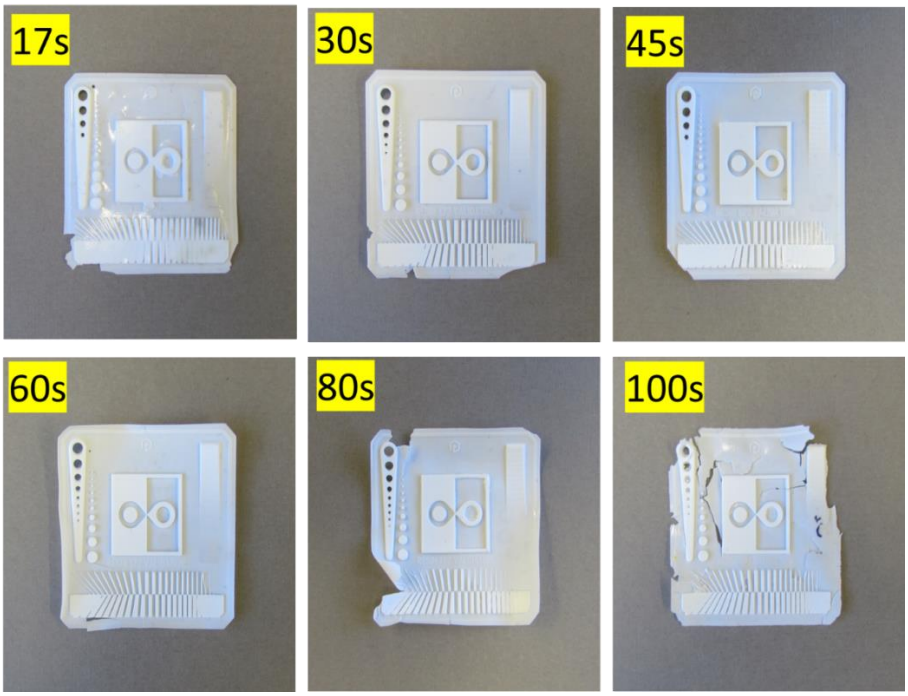

Figure 16: Validation matrices printed at varying exposure times.

A validation matrix used in tandem with ultrasonic verification of the degree of conversion could be used to determine optimal curing parameters. These two techniques could assist in determining optimal exposure times, particularly for mass manufacturing purposes in which time must be reduced to reduce manufacturing cost as much as possible while not critically affecting the DC, mechanical properties, or surface quality.

A weakness of photopolymer additive manufacturing techniques is its limitation of light penetration depth. Solidification starts at the resin surface, which is the surface closest to the

light source, during the polymerization process and continues till it stops due to the attenuation of light through the resin. The depth to which light travels through the resin is known as the cure depth. This phenomenon is described by the Beer-Lambert law, which states the absorbance of a material is proportional to the concentration of the solution and the length of the light path [37]. Light attenuation is especially prevalent in photopolymer resins with fillers, such as alumina powder [38]. Light scattering and light absorption are the two main mechanisms that hinder cure depth in slurries with solid particles [39]. The particle size and refractive index dictate the extent of the light scattering [40].

3.3 Summary

Ultrasonics were successfully able to observe a change in ultrasonic velocity with respect to changes in curing times. The trend produced was representative of the degree of conversion of the monomers into polymeric chains. The initial FTIR spectroscopy measurements on the UV post processed parts did not indicate a trend in C=C bonds that are associated with the polymerization process for the samples that were UV post processed. The FTIR spectroscopy measurements on the single-layer prints that were not UV post processed indicated a decrease in the associated peaks as exposure time increased. One of the drawbacks of FTIR spectroscopy is the shallow scanning depth of IR light as shown by the inability to show a clear trend in the samples post processed by UV light. This was due to the continued surface polymerization by post processing and exposure to ambient light. When comparing the ability of ultrasonics and FTIR spectroscopy to measure the change in photopolymer DC with respect to changes in printing parameters, ultrasonics has an advantage in its depth of detection. Unlike FTIR which scans the surface with very shallow penetration, ultrasonics probe the entirety of the part that is between the transducers.

4 Mechanical Properties using Ultrasonics

4.1 Intro

Young's modulus of elasticity is an important mechanical property of materials and is defined as a material's resistance to elastic deformation [41]. Typically to obtain the Young's modulus of elasticity of a part, the part must be subjected to large forces that may damage or destroy it. Using a load frame, a force is applied to the part to obtain the stress and strain of the material until failure, and from this data, the Youngs modulus can be calculated. Some of the major downsides associated with mechanical testing are the size and price of the testing equipment, the limitation in sample size and geometry, failure at defects, and the damage or destruction of the part. The elastic modulus of a material can be found nondestructively using acoustics if the material is isotropic and the shear wave velocity, longitudinal wave velocity, and density of the material are known [31]. This section describes a non-destructive ultrasonic technique to test additively manufactured polymer ceramic composites and its viability as an alternative to mechanical testing.

4.2 Results and Discussion

4.2.1 Isotropy Validation

The elastic modulus can be determined using ultrasonics only if the material being tested is isotropic [42]. Several AM methods, such as fused deposition modeling (FDM), produce parts that are anisotropic. FDM printers extrude thermoplastic in layers, this creates mechanical adhesion between the layers [43]. The layers are never fully adhered to one another, and voids occur due to the rounded lines from the filament. For this reason, voids are a natural occurrence, and the mechanical properties of the part are dependent on the orientation of the print [44]. Parts printed with FDM are strongest in the direction of deposition and weak where the layers are

bonded [43]. Theoretically, vat polymerization processes produce parts that are isotropic due to the chemical bonds that make up the layers [43]. The surface of the layers is not fully polymerized and is left in a semi-reacted state, this allows for the subsequent layer to form chemical bonds with each other. Covalent bonds are formed in the X, Y, and Z planes so theoretically the part should be isotropic and fully dense [43].

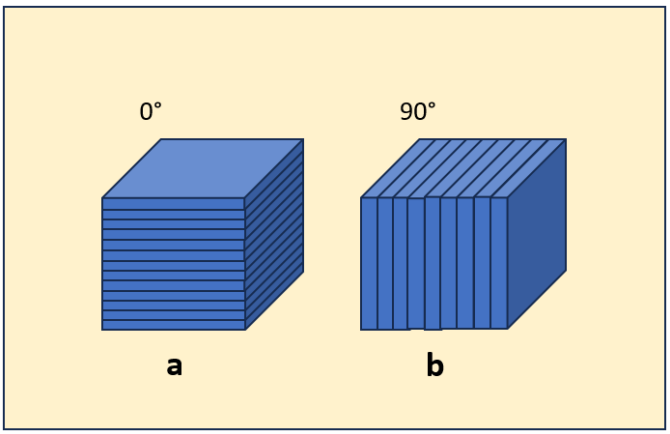

Figure 17: Print orientation diagram: (a) printed 0° to the build plate (b) printed 90° to the build plate.

To validate this claim, two parts are printed with different print orientations and tested using the ultrasonic velocity test. If layer separation or voids are present due to the change of layer orientation, the acoustic attenuation and mechanical properties would differ thus resulting in inconsistent acoustic velocity. The Form 3 SLA printer using Clear resin was used for its simplicity and because it is similar enough to DLP in its printing process to be used as a substitute for this test. Two 7.5 x 7.5 x 5 mm rectangular prisms were printed, one with a 0° print orientation and the second with a 90° print orientation with respect to the build plate, as demonstrated in Figure 17. The printed parts were tested using the setup explained in section 3.1.2.1. The ultrasonic velocity of the parts was calculated and a percent difference of 1.3% was

determined between the two samples. The ultrasonic testing supports the vat polymerization claim of isotropy, and the samples were determined to be isotropic.

Table 1: Samples printed at different orientations.

Sample	Print Orientation	Thickness (m)	ToF (s)	Velocity (m/s)
a	0°	0.006896	0.00000689	2361
b	90°	0.007176	0.000003	2392

4.2.2 Ultrasonic Frequency Sweep

The samples were tested across a frequency range with both longitudinal and shear wave transducers. The frequency sweep range was dependent on the sample and the transducers used. The frequency ranges for the shear wave transducer were generally lower than those of the longitudinal due to the inherent weakness of the shear waves. For materials that possess a large Poisson's ratio, shear waves propagate much slower than longitudinal waves [45]. The speed of the shear acoustic waves was observed to be roughly half the velocity of the longitudinal waves for the materials tested. At higher frequencies, the shear waves experienced a high amount of attenuation and were not able to be successfully recorded. Higher frequency waves generally tend to attenuate more than those of low frequency because of the increased interaction with the medium. Frequency is inversely proportional to the wavelength, the shorter the wavelength the more attenuation the waves experience due to absorption and scattering from particles in the medium [46].

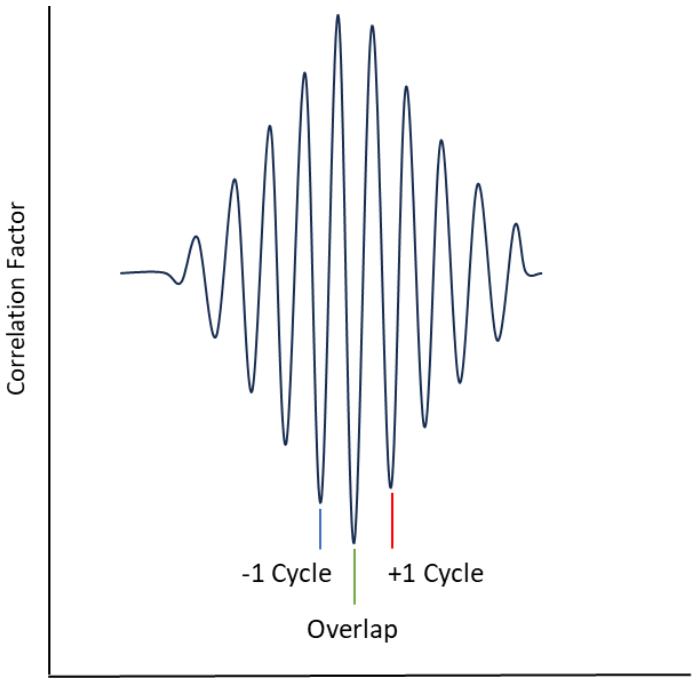

Figure 18: Correlation overlap diagram.

Each frequency tested yielded a correlation result similar to Figure 11. The center peak of the correlation plot is the overlap where the correlation of the two signals is the highest and the peaks adjacent to the center overlap are the offset cycles (illustrated in Figure 18). Three data points were plotted from each frequency tested, the overlap, the offset cycle to the right, and the offset cycle to the left. The data points were plotted, and a line was extrapolated to zero (shown in Figure 19). The y-intercept for the overlap line is the ToF, the intercept for the offset cycles helps to determine the margin of error.

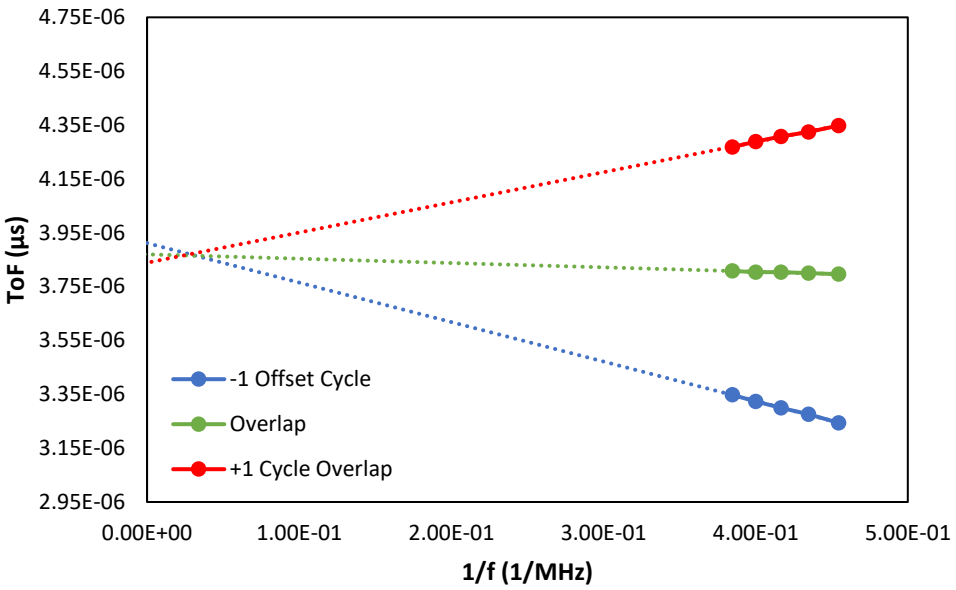

Figure 19: Time of flight through a sample using a frequency sweep.

This method using a frequency sweep can more accurately determine the ToF when compared to the method described in section 3.1.2.1, which only uses a single frequency. Increased accuracy was needed for this technique to determine the material's properties as accurately as possible. The resistance of the wires and transducers was determined by measuring the time of flight of the test setup without a sample. The calculated resistances were subtracted from the resulting time of flight through to the samples to decouple impedances from the setup.

4.2.3 Mechanical Properties Using Ultrasonics

The frequency sweep cross-correlation data was used in Equation 2 to calculate both the shear and the longitudinal velocities. The calculated acoustic velocities were entered in Equation 3 to obtain Poisson's ratio, where V_S is the shear velocity and V_L is the longitudinal velocity. The Poisson ratio is then used the calculate Young's modulus using Equation 4 where v is the Poisson ratio and ρ is the density of the material obtained using the Archimedes test.

$$v = \frac{1 - 2\,(V_S/V_L)^2}{2 - 2\,(V_S/V_L)^2}$$

Equation 4: Acoustic velocity through a material.

$$E = \frac{V_L * \rho(1 + v)(1 - 2v)}{1 - v}$$

Equation 5: Correlation function.

The calculated average values for the elastic modulus and Poisson's ratio for the test samples are listed in Table 4. A 99% copper block standard was tested and compared with data tables in order to validate the technique. The values calculated for the Poisson ratio and Young's modulus, 0.3317± 0.01 and 126.31± 0.2 GPa respectively, had less than a 3% error compared to the values obtained from the data tables for copper.

Table 2: Average mechanical properties using ultrasonics.

Sample Type	Poisson's Ratio	Elastic Modulus by Acoustics (GPa)
Cu	0.3317± 0.01	126.31± 0.2
Formlabs Clear	0.3356± 0.01	4.258± 0.2
20% Alumina	0.3895± 0.01	2.545± 0.1
40% Alumina	0.3716± 0.01	3.991± 0.5

4.2.4 Mechanical Testing

Compression testing was applied to the samples to obtain the mechanical properties of the materials. Brittle materials, like ceramics and ceramic composites, are often used in applications where the material is subjected to compressive loads, therefore its integrity under

these forces is critical [47]. The American Society for Testing and Materials (ASTM) standard D395 was employed for compression testing of the samples. An Epsilon ONE® optical extensometer was used to measure the material deformation to determine the strain, shown in Figure 20. The values for stress and strain for each sample set were plotted (Figure 21) and the elastic modulus was calculated using the Bluehill® Universal software from Instron®.

Figure 20: Compression testing of samples and strain measurement using laser optical elastometer.

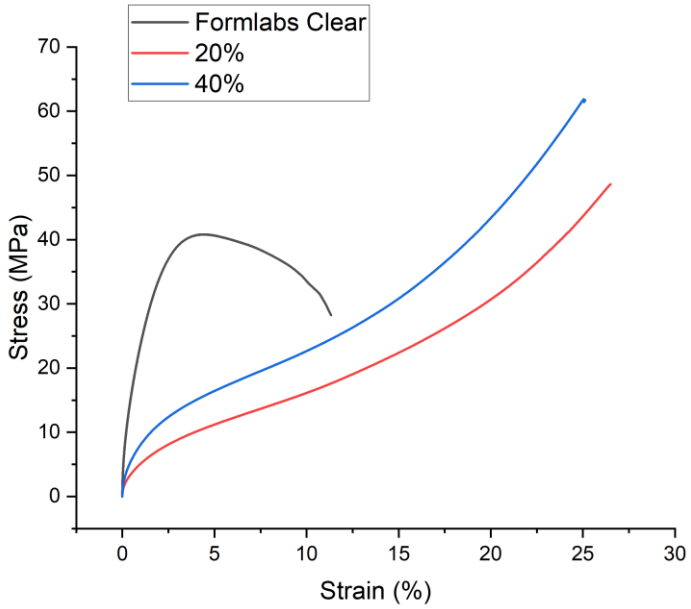

Figure 21: Stress and strain data from mechanical testing of samples.

The mechanical testing results shown in Table 6 were compared with the results calculated using ultrasonics in Table 5. Figure 22 shows a comparison of the elastic modulus obtained using both methods. The Formlabs Clear parts showed only a 4% difference between the values calculated by ultrasonic and compression testing. A 73% difference between the techniques when testing the 20% by weight filler samples and an 84% difference for the 40% by weight filler samples.

Table 3: Average mechanical properties using mechanical compression testing.

Sample Type	Elastic Modulus by Mech Testing (GPa)
Formlabs Clear	4.476± 0.4
20% Alumina	1.162± 0.05
40% Alumina	1.588± 0.5

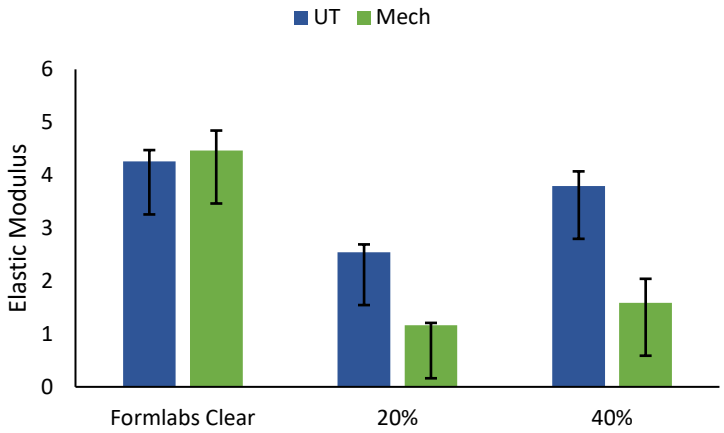

Figure 22: Comparing the elastic modulus values ultrasonics and mechanical testing.

The ultrasonic technique to obtain Young's modulus was only successful in calculating the values within a reasonable margin of error for the homogenous materials. UT failed to obtain comparable modulus values with those obtained by mechanical testing for the composite samples. This technique is determined not suitable for heterogeneous materials like the 20 wt.% and 40 wt.% polymer-ceramic parts. The presence of the ceramic particles may have affected the transmission of the sound waves traveling through the parts due to the interface between the polymer matrix and the ceramic particle [48]. The ceramic particles and the photopolymer have different material properties such as density and acoustic impedance. These differences along with the shape of the particle influence the attenuation, transmission, reflection, and refraction that the wave experiences through the media [48].

4.3 Summary

Ultrasonics were successfully able to calculate Young's modulus for the copper standard and the Formlabs Clear resin. The resulting values for the 20% and 40% polymer composites using ultrasonics did not reflect the values obtained using mechanical compression testing. The technique described shows the ability to accurately calculate the elastic modulus values for

homogeneous materials. Heterogeneous materials introduce interfaces that affect the wave as it passes through the material. The interference between the polymer and ceramic particles negatively affects the propagation of the ultrasonic waves.

5 Conclusion

This work explored ultrasonic techniques to analyze and characterize additively manufactured components. Polymer-ceramic composite samples were manufactured using vat polymerization additive manufacturing processes. The manufactured samples were tested using FTIR spectroscopy, compressive mechanical testing, and ultrasonic testing to verify the effectiveness of ultrasonics in determining the degree of conversion and the modulus of elasticity of the samples. The utilization of ultrasonics proved to be successful in detecting variations in the acoustic velocity of the photopolymer with respect to the changes in exposure time to produce a trend reflective of the degree of monomer conversion. The technique described was capable of probing the sample to find the DC of the entire part, demonstrating superior scanning depth over FTIR, and successfully computing Young's modulus for homogeneous materials. However, ultrasonics encountered limitations when dealing with heterogeneous composites and failed to obtain results consistent with mechanical test data due to parts due to the interface between the polymer matrix and the ceramic particle. Despite this, ultrasonic testing has shown promising results as a non-destructive tool to aid the field of additive manufacturing when used in conjunction with traditional testing techniques.

References

[1] N. Caluk, G. Seisdedos, and A. Azizinamini, "Destructive and non-destructive testing of potential lunar polymer concrete for future lunar habitable infrastructure," *Construction and Building Materials*, vol. 405, pp. 133395–133395, Nov. 2023, doi: https://doi.org/10.1016/j.conbuildmat.2023.133395.

[2] T. Duda and L. V. Raghavan, "3D Metal Printing Technology," *IFAC-PapersOnLine*, pp. 103–110, 2016, doi: https://doi.org/10.1016/j.ifacol.2016.11.111.

[3] A. S. K. Kiran *et al.*, "Additive manufacturing technologies: an overview of challenges and perspective of using electrospraying," *Nanocomposites*, vol. 4, no. 4, pp. 190–214, Oct. 2018, doi: https://doi.org/10.1080/20550324.2018.1558499.

[4] A. Perrot and S. Amziane, "3D Printing in Concrete: General Considerations and Technologies," *John Wiley & Sons, Inc. eBooks*, pp. 1–40, Apr. 2019, doi: https://doi.org/10.1002/9781119610755.ch1.

[5] A. Bagheri and J. Jin, "Photopolymerization in 3D Printing," *ACS Applied Polymer Materials*, vol. 1, no. 4, pp. 593–611, Feb. 2019, doi: https://doi.org/10.1021/acsapm.8b00165.

[6] C. J. Hansen, A. M. Peterson, and J. Park, "3D printing," *Elsevier eBooks*, pp. 1021–1043, Jan. 2022, doi: https://doi.org/10.1016/b978-0-12-821632-3.00017-8.

[7] E. Andrzejewska, "Free-radical photopolymerization of multifunctional monomers," *Three-Dimensional Microfabrication Using Two-Photon Polymerization*, pp. 77–99, 2020, doi: https://doi.org/10.1016/b978-0-12-817827-0.00002-3.

[8] Z. Tarle and M. Par, "Degree of Conversion," *Dental Composite Materials for Direct Restorations*, pp. 63–85, Aug. 2017, doi: https://doi.org/10.1007/978-3-319-60961-4_5.

[9] J. L. Ferracane and E. H. Greener, "The effect of resin formulation on the degree of conversion and mechanical properties of dental restorative resins," *Journal of Biomedical Materials Research*, vol. 20, no. 1, pp. 121–131, Jan. 1986, doi: https://doi.org/10.1002/jbm.820200111.

[10] J. Li, H. Li, A. S. L. Fok, and D. C. Watts, "Multiple correlations of material parameters of light-cured dental composites," *Dental Materials*, vol. 25, no. 7, pp. 829–836, Jul. 2009, doi: https://doi.org/10.1016/j.dental.2009.03.011.

[11] S. Laurenson, "DLP 3D Printing: Understanding process and materials enables you to prevent production problems," *Wevolver*, Nov. 2019. https://www.wevolver.com/article/dlp.3d.printing.understanding.process.and.materials.enables.you.to.prevent.production.problems

[12] J. Wu *et al.*, "Evolution of material properties during free radical photopolymerization," *Journal of the Mechanics and Physics of Solids*, vol. 112, pp. 25–49, Mar. 2018, doi: https://doi.org/10.1016/j.jmps.2017.11.018.

[13] D. Salamon, "Advanced Ceramics," *Advanced Ceramics for Dentistry*, pp. 103–122, 2014, doi: https://doi.org/10.1016/b978-0-12-394619-5.00006-7.

[14] F. Pawel, M. Rozmus, and B. Smuk, "Properties of alumina ceramics obtained by conventional and non-conventional methods for sintering ceramics," *Journal of Achievements of Materials and Manufacturing Engineering*, vol. 48, pp. 29–34, Sep. 2011.

[15] P. Auerkari, *Mechanical and physical properties of engineering alumina ceramics*. Espoo: Technical Research Centre Of Finland, 1996.

[16] A. J. Ruys, *Alumina Ceramics : Biomedical and Clinical Applications*. Duxford, United Kingdom: Woodhead Publishing, 2019.

[17] B. L. Krasnyi, V. P. Tarasovskii, E. V. Rakhmanova, and V. V. Bondar', "Chemical Resistance of Ceramic Materials in Acids and Alkalis," *Glass and Ceramics*, vol. 61, no. 9/10, pp. 337–339, Sep. 2004, doi: https://doi.org/10.1023/b:glac.0000048706.05368.71.

[18] V. Hauk, *Structural and Residual Stress Analysis by Nondestructive Methods*. Elsevier, 1997.

[19] S. Rasaki, D. Xiong, S. Xiong, F. Su, M. Idrees, and Z. Chen, "Photopolymerization-based additive manufacturing of ceramics: A systematic review," *Journal of Advanced Ceramics*, vol. 10, no. 3, pp. 442–471, Mar. 2021, doi: https://doi.org/10.1007/s40145-021-0468-z.

[20] V. Truxova, J. Safka, M. Seidl, I. Kovalenko, L. Volensky, and M. Ackermann, "CERAMIC 3D PRINTING: COMPARISON OF SLA AND DLP TECHNOLOGIES," *MM Science Journal*, vol. 2020, no. 2, pp. 3905–3911, Jun. 2020, doi: https://doi.org/10.17973/mmsj.2020_06_2020006.

[21] O. Santoliquido, F. Camerota, A. Rosa, and A. Ortona, "A novel device to simply 3D print bulk green ceramic components by stereolithography employing viscous slurries," *Open Ceramics*, vol. 5, p. 100089, Mar. 2021, doi: https://doi.org/10.1016/j.oceram.2021.100089.

[22] S. K. Dwivedi, M. Vishwakarma, and Prof. Akhilesh. Soni, "Advances and Researches on Non Destructive Testing: A Review," *Materials Today: Proceedings*, vol. 5, no. 2, pp. 3690–3698, 2018, doi: https://doi.org/10.1016/j.matpr.2017.11.620.

[23] S. Kumar and D. G. Mahto, "Recent Trends in Industrial and Other Engineering Applications of Non Destructive Testing: A Review," *International Journal of Scientific & Engineering Research*, vol. 4, no. 9, Sep. 2013.

[24] X. Wang, H. Xie, Y. Tong, B. Wang, and H. Hu, “Three-point bending properties of 3D_C/C_TiC_Cu composites based on acoustic emission technology,” *Mechanical Systems and Signal Processing*, vol. 184, pp. 109693–109693, Feb. 2023, doi: https://doi.org/10.1016/j.ymssp.2022.109693.

[25] C. Pantea *et al.*, “Digital ultrasonic pulse-echo overlap system and algorithm for unambiguous determination of pulse transit time,” *Review of Scientific Instruments*, vol. 76, no. 11, Nov. 2005, doi: https://doi.org/10.1063/1.2130715.

[26] D.W. Van Krevelen and K. te Nijenhuis, “Acoustic Properties,” *Elsevier eBooks*, pp. 505–522, Jan. 2009, doi: https://doi.org/10.1016/b978-0-08-054819-7.00014-5.

[27] “BYK-W 9010,” *www.byk.com*. https://www.byk.com/en/products/additives-by-name/byk-w-9010 (accessed Sep. 18, 2023).

[28] “Organic phosphoric acid esters,” *www.schaerer-surfactants.com*. https://www.schaerer-surfactants.com/en/products/organic-phosphoric-acid-esters (accessed Aug. 16, 2023).

[29] “Genesis Development Resin Base – liter | Tethon 3D,” *tethon3d*, Nov. 16, 2016. https://tethon3d.com/product/genesis/ (accessed Sep. 09, 2023).

[30] OpenStax, “11.7 Archimedes’ Principle,” *pressbooks.online.ucf.edu*, Aug. 2016, Available: https://pressbooks.online.ucf.edu/phy2053bc/chapter/archimedes-principle/

[31] Juan Antonio García-Manrique *et al.*, “Study of the Degree of Cure through Thermal Analysis and Raman Spectroscopy in Composite-Forming Processes,” *Materials*, vol. 12, no. 23, pp. 3991–3991, Dec. 2019, doi: https://doi.org/10.3390/ma12233991.

[32] “Correlation Coefficient,” *www.jmp.com*. https://www.jmp.com/en_us/statistics-knowledge-portal/what-is-correlation/correlation-coefficient.html

[33] S. P. Davtyan and A. O. Tonoyan, “The Frontal Polymerization Method in High Technology Applications,” *Review journal of chemistry*, vol. 9, no. 1, pp. 71–94, Jan. 2019, doi: https://doi.org/10.1134/s2079978018040039.

[34] D. S. Achilias, “A Review of Modeling of Diffusion Controlled Polymerization Reactions,” *Macromolecular Theory and Simulations*, vol. 16, no. 4, pp. 319–347, May 2007, doi: https://doi.org/10.1002/mats.200700003.

[35] J. Huang, P. Fu, W. Li, L. Xiao, J. Chen, and X. Nie, “Influence of crosslinking density on the mechanical and thermal properties of plant oil-based epoxy resin,” *RSC Advances*, vol. 12, no. 36, pp. 23048–23056, 2022, doi: https://doi.org/10.1039/D2RA04206A.

[36] “Q: How deep does the infrared light penetrate at the position of contact between the prism and sample during ATR measurements?,” *www.shimadzu.com*.

https://www.shimadzu.com/an/service-support/technical-support/ftir/faq/atr.html (accessed Nov. 30, 2023).

[37] J. Clark, "The Beer-Lambert Law," *Chemistry LibreTexts*, Jan. 30, 2023. https://chem.libretexts.org/Bookshelves/Physical_and_Theoretical_Chemistry_Textbook_Maps/Supplemental_Modules_(Physical_and_Theoretical_Chemistry)/Spectroscopy/Electronic_Spectroscopy/Electronic_Spectroscopy_Basics/The_Beer-Lambert_Law

[38] G. Fei, C. Parra-Cabrera, K. Zhong, M. L. Tietze, K. Clays, and R. Ameloot, "Scattering Model for Composite Stereolithography to Enable Resin–Filler Selection and Cure Depth Control," *ACS applied polymer materials*, vol. 3, no. 12, pp. 6705–6712, Nov. 2021, doi: https://doi.org/10.1021/acsapm.1c01519.

[39] S. Zakeri, M. Vippola, and E. Levänen, "A comprehensive review of the photopolymerization of ceramic resins used in stereolithography," *Additive Manufacturing*, vol. 35, p. 101177, Oct. 2020, doi: https://doi.org/10.1016/j.addma.2020.101177.

[40] E. Stefan, T. Didriksen, Tor, M. Fontaine, Henrik Ræder, and Per Martin Rørvik, "Effects of powder properties on the 3D printing of BaTiO3 ceramic resins by stereolithography," *Progress in Additive Manufacturing*, vol. 8, no. 6, pp. 1641–1651, Mar. 2023, doi: https://doi.org/10.1007/s40964-023-00431-w.

[41] D. R. H. Jones and M. F. Ashby, "Elastic Moduli," *Engineering Materials 1*, pp. 31–47, 2019, doi: https://doi.org/10.1016/b978-0-08-102051-7.00003-8.

[42] G. Seisdedos *et al.*, "Assessment and Non-Destructive Evaluation of the Influence of Residual Solvent on a Two-Part Epoxy-Based Adhesive Using Ultrasonics," *Applied sciences*, vol. 13, no. 6, pp. 3883–3883, Mar. 2023, doi: https://doi.org/10.3390/app13063883.

[43] "Validating Isotropy in SLA 3D Printing," *Formlabs*. https://formlabs.com/blog/isotropy-in-SLA-3D-printing/

[44] M. R. Khosravani, F. Berto, M. R. Ayatollahi, and T. Reinicke, "Characterization of 3D-printed PLA parts with different raster orientations and printing speeds," *Scientific Reports*, vol. 12, no. 1, Jan. 2022, doi: https://doi.org/10.1038/s41598-022-05005-4.

[45] A. O. Oyelade, N. O. Obaji, and C. V. Agbaeze, "Longitudinal and shear waves propagation in a periodic foundation with negative Poisson's ratio," *Forces in Mechanics*, vol. 4, p. 100035, Oct. 2021, doi: https://doi.org/10.1016/j.finmec.2021.100035.

[46] W. Alex Mason and H. J. McSkimin, "Attenuation and Scattering of High Frequency Sound Waves in Metals and Glasses," vol. 19, no. 3, pp. 464–473, May 1947, doi: https://doi.org/10.1121/1.1916504.

[47] " What is Compression Testing? An Introduction," *www.intron.com*. https://www.instron.com/en/resources/test-types/compression-test

[48] J. Chang, C. Zheng, and Q.-Q. Ni, “The ultrasonic wave propagation in composite material and its characteristic evaluation,” *Composite Structures*, vol. 75, no. 1–4, pp. 451–456, Sep. 2006, doi: https://doi.org/10.1016/j.compstruct.2006.04.040.
.

Vita

Christian Alexander Ruiz was born and raised in El Paso Texas. Christian joined the University of Texas at El Paso in August 2017 to pursue a Bachelor of Science in Mechanical Engineering. In October 2020 he began working under Dr. Yirong Lin as an undergraduate research assistant with support from the Polymer Partnership for Research Education Consortium in Ceramics and Polymers (PRE-CCAP). Christian graduated with his bachelor's in December 2021 after which he started at Los Alamos National Laboratory, first as a post-bachelor researcher and then as a graduate research assistant. Christian started his Master of Science in Mechanical Engineering at the University of Texas at El Paso in August 2022 as he continued to work at Los Alamos National Laboratory as a graduate research assistant.